Journal of Alloys and Compounds 509 (2011) 7078–7086

Contents lists available at ScienceDirect

Journal of Alloys and Compounds

journal homepage: www.elsevier.com/locate/jallcom

Precipitation behavior of μ phase and creep rupture in single crystal superalloy CMSX-4

KuiYu Cheng[a,b,*], ChangYong Jo[b], Tao Jin[a], ZhuangQi Hu[a]

[a] Superalloy Division, Institute of Metal Research, Chinese Academy of Sciences, Shenyang 110016, China
[b] High Temperature Materials Group, Korea Institute of Materials Science, Changwon 641-010, Republic of Korea

ARTICLE INFO

Article history:
Received 6 June 2010
Received in revised form 30 March 2011
Accepted 1 April 2011
Available online 7 April 2011

Keywords:
Nickel-base single crystal superalloy
Topologically close packed phase
Thermal exposure
Creep

ABSTRACT

Precipitation behavior of a topologically close packed (TCP) μ phase as well as its role during the creep deformation in single crystal superalloy CMSX-4 have been investigated. The μ particles nucleated and grew based on low index planes of both the μ phase ($\{1\,1\,\bar{2}\,0\}$ and $\{1\,0\,\bar{1}\,0\}$) and the matrix ($\{1\,1\,0\}$, $\{0\,0\,1\}$ or $\{1\,1\,1\}$ and $\{1\,1\,2\}$) by epitaxial growth toward $\langle 0\,0\,0\,1\rangle_\mu$ or $\langle 1\,1\,0\rangle_\gamma$ directions, which predominantly resulted in a rod-like morphology. Interestingly, composition of these rod-like μ particles varied with the ratio of Ni/(W + Re) due to the different diffusion rates of these elements in the matrix during thermal exposure. Moreover, the γ′ evolution played an important role in the precipitation behavior and the fracture behavior of the μ phase. The rod-like μ particles were not fractured by stress concentration, as they were surrounded by the γ′ envelope.

1. Introduction

The nickel-base superalloys are applied in the crucial parts of aero-gas turbine engines, thereby having been drawing extensive research over many various fields of study [1–6]. These alloys can operate for thousands of hours at temperatures as high as 1100 °C due to in particular their high temperature creep resistance [6]. The high temperature creep properties of recently developed nickel-base single crystal superalloys are mainly improved by introducing large amount of the refractory elements such as Mo, Re and W [7–11], although excessive amount of these elements may render the alloy prone to topologically close-packed phases, such as σ-, μ-, P- or R-phase [4–18]. Presence of these phases can seriously deteriorate the high temperature mechanical properties of superalloys [7–17]. Firstly, formation of these TCP phases can lead to the depletion of solid solution strengthening elements in the matrix, which becomes more effective in creep conditions and results in severe reduction of the stress rupture life at high temperature [12,13]. At the same time, these brittle phases can also serve as damage accumulation sites and disrupt the regularity of the γ/γ′ microstructure [13].

Compared to the other TCP phases, the μ phase in particular is under the hottest debate, as it presents various morphologies in superalloys and does not always affect the high temperature creep properties of superalloys [12,14–17]. Recently, Tian et al. reported that Re has an obvious effect on the precipitated morphology of μ phase during stress/free-stress aging and the strip-like μ phase promotes the initiation and propagation of the cracks to accelerate the lifetime deterioration of 6% W alloy, while the sphere-like μ phase formed in 4.5% Re alloy have the double roles of both weakening creep resistance and hindering dislocation movement during creep [12]. In Wang et al.'s work, it also shows little adverse effect of the blocky μ phase on the creep properties of a direction solidified superalloy [14]. To some extent, therefore, the high temperature mechanical properties are dependant on morphologies of the μ phase. The morphology and precipitation behavior of the μ phase are mainly determined by the interface coherency between it and the γ/γ′ matrix [3,5]. Besides, the μ-phase precipitates semi-coherently with the matrix, which may explain its strong influence on the surrounding microstructure. However, le Graverend et al.'s FEM model shows that the μ phase induced stress fields do not seem to be responsible for the modification of the γ′-rafted orientation over a long range beyond the μ-needles [5].

This paper was concerned with the well known second generation single crystal superalloy CMSX-4. Since the CMSX-4 alloy was verified as a μ phase stable alloy [18], it is advantageous to study the precipitation behavior of the μ phase and its role during creep deformation without influence from the other TCP phases. The present study is focused on displaying the crystallographic orientation relationship between a rod-like μ phase and the matrix and how it can affect the precipitation behavior of this rod-like μ phase and the subsequent mechanical properties of the alloy. In

* Corresponding author at: High Temperature Materials Group, Korea Institute of Materials Science, Changwon 641-010, Republic of Korea. Tel.: +82 55 2803308; fax: +82 55 2803492.
E-mail address: kuiyucheng@hotmail.com (K. Cheng).

0925-8388/$ – see front matter © 2011 Elsevier B.V. All rights reserved.
doi:10.1016/j.jallcom.2011.04.001

Table 1
Chemical composition of CMSX-4 alloy (wt.%).

Alloy	Co	Cr	W	Al	Ti	Ta	Mo	Re	Hf	Ni
CMSX-4	9.8	6.5	6.0	5.6	1.0	6.5	0.6	3.0	0.1	bal.

addition, the strong interface strength between the μ phase and γ/γ′ matrix may not be the only reason for unfavorable crack initiation from the μ phase during creep deformation. Transformation of the μ phase due to γ′ evolution was considered as well in the present study, on which the possible fracture manner of μ phase during creep deformation was discussed. The influence of different alloying elements on the TCP phase formation was also discussed.

2. Experimental

The single crystal superalloy CMSX-4 used in the present work was supplied by the Cannon-Muskegon Corporation and cast by Bridgman method into the form of 14 mm diameter rods with an approximate length of 220 mm. Each bar had a ⟨0 0 1⟩ crystallographic orientation within a few degrees of its long axis. The composition is listed in Table 1. All the CMSX-4 single crystal bars were firstly given a standard heat treatment procedure (heated to 1260 °C at 360 °C/h, held for 0.2 h, heated to 1288 °C at 30 °C/h and heated to 1320 °C at 2 °C/h, held for 2 h, AC + 1140 °C/2 h, AC + 870 °C/20 h, AC; subsequently described as the HT specimen) resulting in a homogeneous distribution of cuboidal γ′ particles (70 vol.%) aligned along the ⟨0 0 1⟩ directions with a mean edge size of 450 nm [19].

The HT specimens were thermally exposed at 1050 °C for 125–5000 h and 950 °C for 500–5000 h, respectively. Then the creep tests at 1050 °C and 165 MPa were performed on the specimens with and without thermal exposure to study the role of the μ phase during creep deformation. The subsequent microstructures were carefully examined by JSM-5800 and JSM-6700F scanning electron microscopes (SEM) and JEM-2100F transmission election microscope (TEM). Some of the exposed samples were immersed in an electrolyte composed of 10% HCl and 1% tartaric acid in methanol and exposed to an anodic current density for a few minutes to reveal the stereo-morphology of the μ phase, while the others were etched by means of waterless Kalling's reagent. In order to avoid the "composition contamination" from the matrix at most, the μ particles were extracted out of the electrolyzed samples by carbon replica for EDS analysis. Specimens for TEM examination were jet polished using 7% perchloric acid and 3% glycerin in methanol at −20 °C and 40 V. The μ phase was identified and analyzed using selected area diffraction pattern (SADP) and energy dispersive spectroscopy (EDS). SAD patterns obtained in the transmission electron microscopy (TEM) were indexed and compared with the help of the Desktop Microscopist V2.2 software (Lucuna Lab., Beaver ton, OR). Size and volume fraction of the μ particles in thermally exposed specimens were measured and calculated by Imagetool 3.00. The length, width and thickness of the μ particles were measured manually in at least five photos taken from each condition. As the μ particles in the present study are mostly rod-like rather than plate-like, the volume fraction was obtained by the product of area fraction and line fraction. Firstly, the μ particles were selected in the photo by the software automatically due to the contrast and afterwards the fine selection was done manually, which gives the area fraction. Secondly, random lines were made across the selected areas and then the line fraction was obtained by the ratio of the sections to the length of all random lines. This procedure was repeated at each condition until the volume fraction results appeared to be relatively stable.

3. Results

3.1. Temperature dependence of the μ phase precipitation

In samples annealed at 950 °C, formation of the μ phase was occasionally detected after 500 h. With increasing exposure time, amount of the μ phase had no obvious change from 1000 h to 3000 h until after 5000 h (Fig. 1).

At 1050 °C (Fig. 2), the μ phase clearly precipitated just after 200 h exposure and the amount of it increased obviously from 200 h to 500 h exposure. With extended thermal exposure from 1000 to 3000 h, amount of the μ phase was relatively constant except that some particles grew dramatically to about 50–150 μm in length. After 5000 h, however, the γ′ phase coarsened immensely, while the μ phase revealed big blocky morphology and obviously decreased in amount. Moreover, it was found that the obvious coarsening of γ′ phase took place after 1000 h at 950 °C and after 200 h at 1050 °C, respectively (Fig. 3), while precipitation of the μ phase revealed obvious increase at corresponding conditions. This implies that the γ′ evolution may affect the precipitation behavior of μ phase. Table 2 summarizes the size and volume fraction of the μ phase in specimens annealed at 950 and 1050 °C. It should be noted that the measurement error of the μ phase size might be very little, while the measurement of volume fraction varied a lot before it became relatively stable.

It can be also found in the micrographs that amount of the μ phase was much larger at 1050 °C than that at 950 °C compared at the same thermal exposure time, while the size did not change as dramatically as the amount. This indicates that nucleation of the μ phase is more sensitive to the given temperatures in the present study than growth of the μ phase. The distinct temperature dependence of nucleation and growth behaviors of μ phase might also be related to the γ′ evolution.

3.2. Macroscopic characterization of the μ phase

As shown in Figs. 1 and 2, the μ particles appeared to have either acicular or blocky morphology when observed on plane sections of $\{0\,0\,1\}_{\gamma}$ regardless of the given temperatures. Also, it shows that some long acicular precipitates were discrete along their lines. To reveal the actual features more clearly, the μ phase was extracted out from the matrix to show the morphology in three dimensions (Fig. 4). The μ particles were mostly rod-like accompanied by a few plates. At 950 °C (Fig. 4a), the rod-like particles seemingly interweaved with each other within a plane which might be the $(1\,1\,1)_{\gamma/\gamma'}$ according to the crystallographic relationship in the micrograph. While at 1050 °C (Fig. 4b), the rod-like particles extruded spatially in the γ/γ′ matrix or interweaved with each

Table 2
Size and volume fraction of μ phase in specimens annealed at 950 and 1050 °C.

	950 °C				1050 °C			
Time (h)	1000	2000	3000	5000	500	1000	2000	3000
Width (μm)	0.1–0.6		0.2–2		0.4–3	1–2.6	1–5	2–8
Thickness (nm)	15–200	20–300		20–400	30–600	50–500		60–800
Length (μm)	<20			4–30	<20	8–50		15–150
Volume fraction	Too low to measure				0.13%	0.11%	0.14%	0.17%

Table 3
Chemical compositions of different positions of plate-like μ particle in specimen annealed at 1050 °C for 750 h.

Position		Co	Cr	Ni	W	Re	Mo	Ta	Ti
Point A	wt.%	8.91	9.05	21.98	32.18	26.04	1.85	–	–
	at.%	14.63	16.83	36.21	16.93	13.53	1.86	–	–
Point B	wt.%	8.90	8.46	39.33	21.58	15.75	0.78	4.74	0.45
	at.%	12.28	13.24	54.49	9.55	6.88	0.66	2.13	0.77

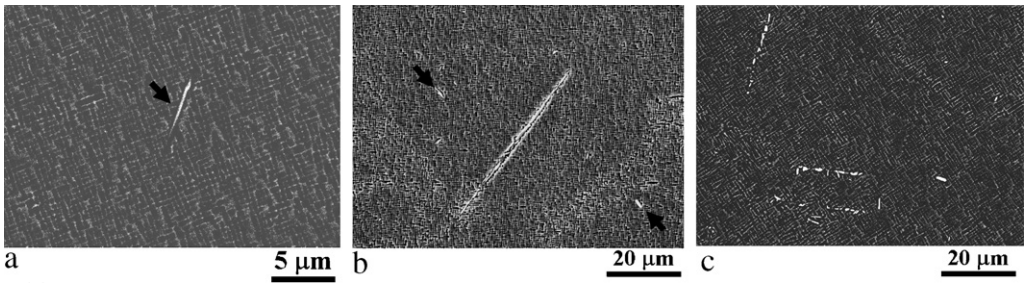

Fig. 1. SEM micrographs of the μ phase precipitation at 950 °C: (a) 500 h, (b) 1000 h and (c) 5000 h. Black arrows indicate the μ particles.

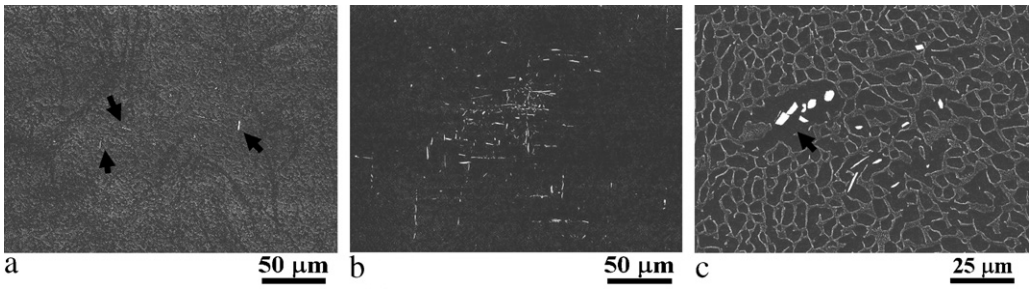

Fig. 2. SEM micrographs of the μ phase precipitation at 1050 °C: (a) 200 h, (b) 500 h and (c) 5000 h. Black arrows indicate the μ particles.

other within several crystallographic planes of the γ/γ′ matrix. Diversity of the growth manner at 1050 °C was due to the relatively high thermodynamic force upon the μ phase at this temperature. Clearly, these interweaved rods within a plane resulted in the aligned segmented appearance when observing from the cross-sectioned plane as shown in Figs. 1 and 2.

The amount of the plate-like μ particles is very low. Some of the plate-like particles, which formed at the early stage of the thermal exposure, were deliberately examined. Interestingly, the planar precipitates consisted of some frameworks connected by thin layers as shown in Fig. 5. In the backscattered electron images, the frameworks are bright while the neighbor thin layers are dark, indicating that the frameworks inside the planar precipitates contain much heavier elements than the thin layers. The EDS analysis (detail in Table 3) of the planar precipitate at 1050 °C clearly shows that the framework (marked by A) consists of higher content of W and Re but lower content of Ni compared with the neighbor thin layer (marked by B). Recently, several authors have speculated on the existence of a planar phase acting as the precursor for other TCP phases [8]. However, since the frameworks and the thin layers simultaneously occurred in the plate-like precipitates during the thermal exposure period, it is difficult to tell which one is the precursor of the other one. Nevertheless, one may say that the μ phase in CMSX-4 alloy has a large shift in composition during the

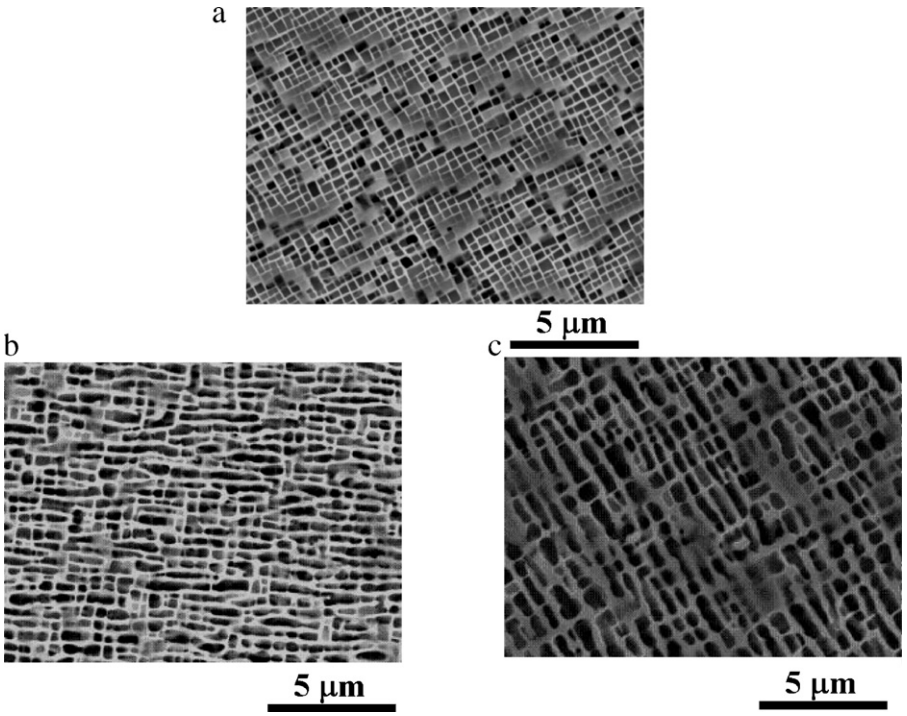

Fig. 3. The onset of obvious γ′ coarsening at 950 °C and 1050 °C, respectively: (a) HT, (b) 950 °C/1000 h and (c) 1050 °C/200 h.

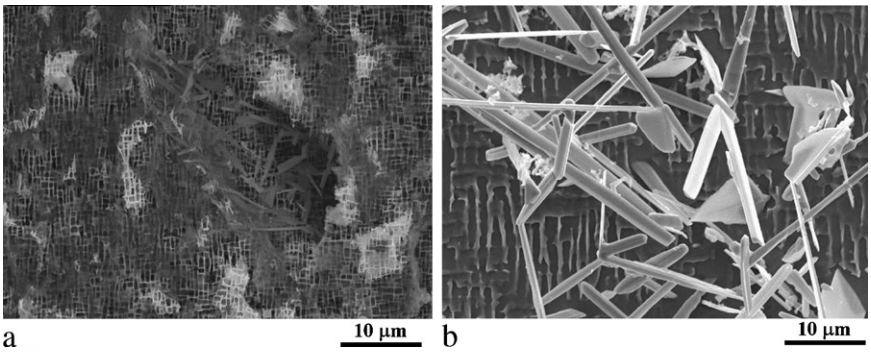

Fig. 4. SEM micrographs show the morphology of the μ phase revealed by stripping away the γ/γ′ at 950 °C and 1050 °C, respectively: (a) 950 °C/2000 h and (b) 1050 °C/2000 h. The μ particles show mainly rod-like at both temperatures.

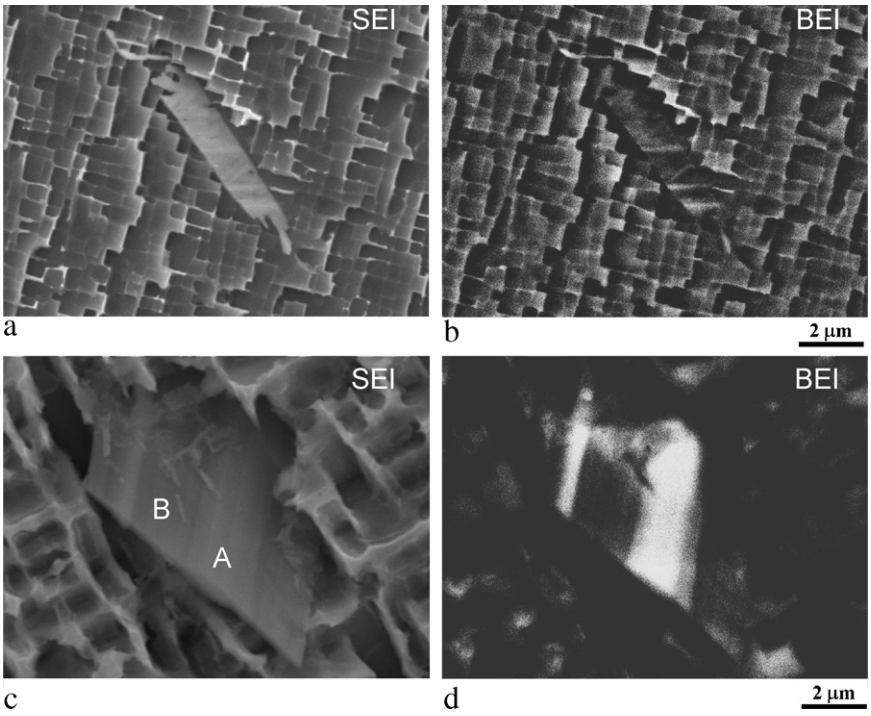

Fig. 5. Secondary electrons images (SEI) and corresponding backscattered electron images (BEI) of the plate-like μ particles at 950 °C and 1050 °C, respectively: (a) 950 °C/800 h, (b) BEI of (a), (c) 1050 °C/750 h and (d) BEI of (c).

precipitation process and the relative large thin layers might form due to the high diffusion rate of Ni [20].

Then, compositions of the μ particles were carefully examined. Thirty μ particles at conditions of 950 °C/1000, 3000 h, 5000 h and 1050 °C/500 h, 3000 h were analyzed and compared to show the statistical composition distribution of the μ phase (Fig. 6). The results are summarized as: (i) the μ phase was mainly composed of Ni, Cr, Co, Re and W, and had a large composition range; (ii) Ni played a contrary role with Re, W and Cr in the contribution to μ phase composition; (iii) with increasing exposure time, Re and W contents increased to substitute for Ni, and Re content gradually approached W content, while the other elements were relatively stable; (iv) compositions of the μ phase reached to equilibrium at 950 °C/3000 h and 1050 °C/500 h respectively with respect to similar element content (Table 3).

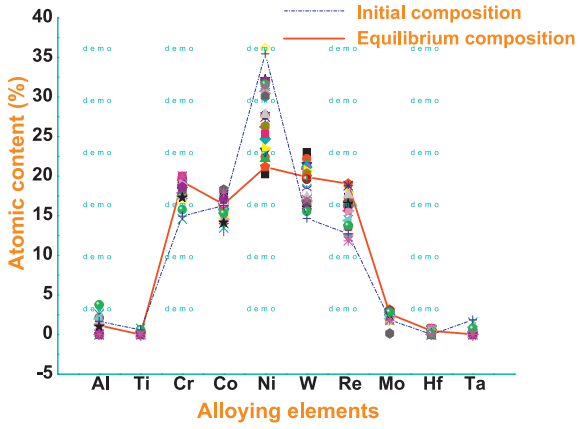

Fig. 6. Statistical distribution of μ phase composition obtained by comparing the compositions of 30 μ particles at conditions of 950 °C/1000 h, 3000 h, 5000 h and 1050 °C/500 h, 3000 h. Note the contrary contribution of Ni and (Re + W) to the μ phase composition.

3.3. Characterization of μ phase

A notable feature of μ phase is the tendency to exhibit twinning and faulting [18]. Fig. 7 shows the typical twinning structure of μ

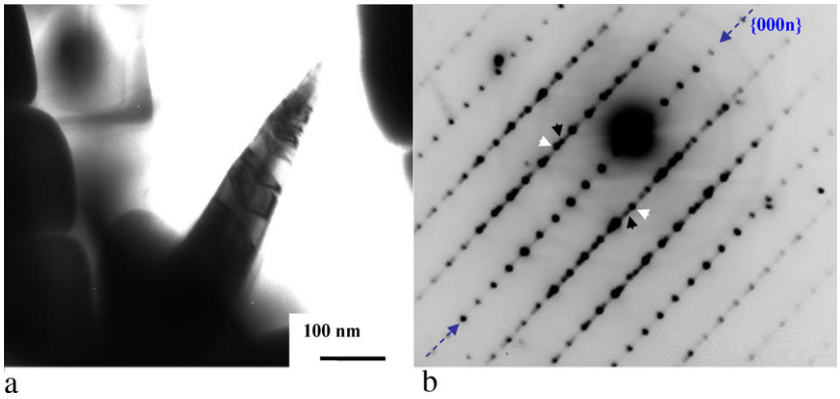

Fig. 7. TEM micrograph (a) of the typical twinned μ phase from 950 °C/1000 h and the corresponding diffraction pattern (b) showing it a {0 0 0 1} type twin at zone axis of $[1\ 1\ \bar{2}\ 0]_{\text{twin }\mu}/[0, 2\ \bar{1}\ 2\ 0]_{\text{twin }\mu}$. Black and red arrows point spots from the twins, while the blue arrows show the spots from twin planes. (For interpretation of the references to color in the figure caption, the reader is referred to the web version of the article.)

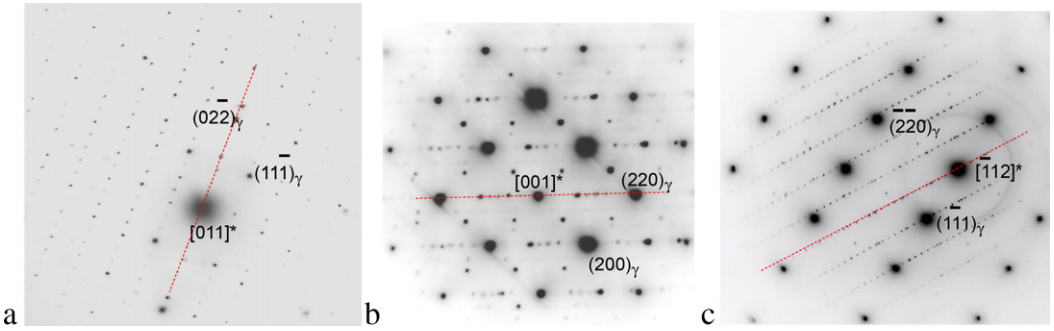

Fig. 8. Representative orientation relationships of the μ phase and the matrix described by three sets of diffraction patterns at zone axis of (a) $[1\ 1\ \bar{2}\ 0]_\mu//[0\ 1\ 1]_\gamma$, (b) $[0\ 1\ \bar{1}\ 0]_\mu//[0\ 0\ 1]_\gamma$ and (c) $[1\ 1\ \bar{2}\ 0]_\mu//[\bar{1}\ 1\ 2]_\gamma$. The red broken lines index the $(0\ 0\ 0\ n)_\mu$. (For interpretation of the references to color in the figure caption, the reader is referred to the web version of the article.)

phase under TEM observation and the corresponding diffraction pattern. Here, the twin plane is parallel to (0 0 0 1) with the diffraction zone axis of $[1\ 1\ \bar{2}\ 0]_{\text{twin }\mu}/[0, 2\ \bar{1}\ 2\ 0]_{\text{twin }\mu}$. This feature is due to the complicated stacking manner of μ phase [21].

Most importantly, the μ phase showed good orientation relationship with the matrix, which can be exclusively summarized to three sets of diffraction patterns as shown in Fig. 8. Then, the corresponding orientation relationship between the μ phase and the matrix was derived and indexed with the help of the Desktop Microscopist V2.2 software as follows:

$$[1\ 1\ \bar{2}\ 0]_\mu//[0\ 1\ 1]_\gamma \quad [0\ 1\ \bar{1}\ 0]_\mu//[0\ 0\ 1]_\gamma \quad [1\ 1\ \bar{2}\ 0]_\mu//[\bar{1}\ 1\ 2]_\gamma$$
$$(0\ 0\ 0\ 1)_\mu//(0\ 1\ \bar{1})_\gamma \quad (0\ 0\ 0\ 1)_\mu//(1\ 1\ 0)_\gamma \quad (0\ 0\ 0\ 1)_\mu//(1\ 1\ 0)_\gamma$$

Interestingly, all the μ precipitates have a common relationship with the matrix, that is $(0\ 0\ 0\ 1)_\mu//(1\ 1\ 0)_\gamma$. Fig. 9 shows the standard diffraction patterns simulated by Desktop Microscopist V2.2 software of μ at [0 0 0 1] zone and of γ/γ′ at [1 1 0] zone, respectively. It can be seen that the low index planes $\{1\ 1\ \bar{2}\ 0\}$ and $\{1\ 0\ \bar{1}\ 0\}$ of μ can keep good crystallographic relationship (parallel) with the low index planes {1 1 0} and {0 0 1} or {1 1 1} and {1 1 2} of the matrix at the same time. Thus, considering that most of the μ precipitates were rod-like and extruded in the matrix, it is tempting to say that the μ phase may nucleate and grow based on the low index planes of both the μ phase and the matrix by epitaxial growth toward $\langle 0\ 0\ 0\ 1\rangle_\mu$ or $\langle 1\ 1\ 0\rangle_\gamma$ directions, which are the close packing directions of the matrix. Apparently, this process is energetically favorable [22]. In this case, possible precipitation mechanisms of the μ phase may be derived as shown in Fig. 10 according to the epitaxy theory in solids [22]:

(i) Epitaxial growth of the μ phase is dependent on one low index plane $(h_1\ k_1\ l_1)$ of the matrix and its $(H_1\ K_1\ i_1\ L_1)$ plane. The μ phase will grow on this plane, but growth in the normal direction n_1 of the $(h_1\ k_1\ l_1)$ will be limited. At times the morphology will present thin plates, which occurred infrequently in this study but can be found frequently elsewhere [8].

(ii) If epitaxial growth of the μ phase is meanwhile dependent on another low index plane $(h_2\ k_2\ l_2)$ of the matrix and its $(H_2\ K_2\ i_2\ L_2)$ plane, the μ phase will grow along the cross-line of $(h_1\ k_1\ l_1)$ and $(h_2\ k_2\ l_2)$ to form rod-like morphology, since the growth in radial directions (n_1 and n_2) of the rod is limited. The rods usually present flat cross sections (see in Fig. 10b),

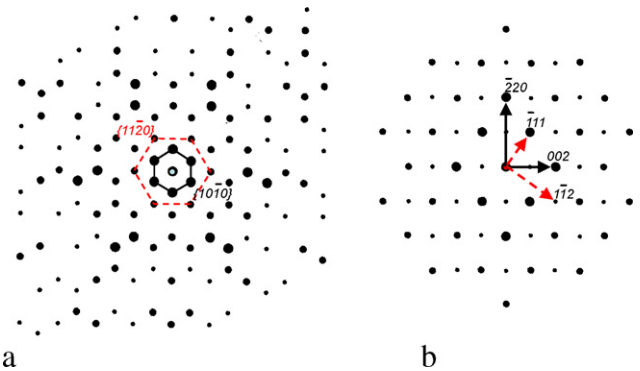

Fig. 9. Standard diffraction patterns simulated by Desktop Microscopist V2.2 software. (a) [0 0 0 1] zone of μ (W_6Fe_7) and (b) [1 1 0] zone of γ/γ′ (Ni/Ni_3Al).

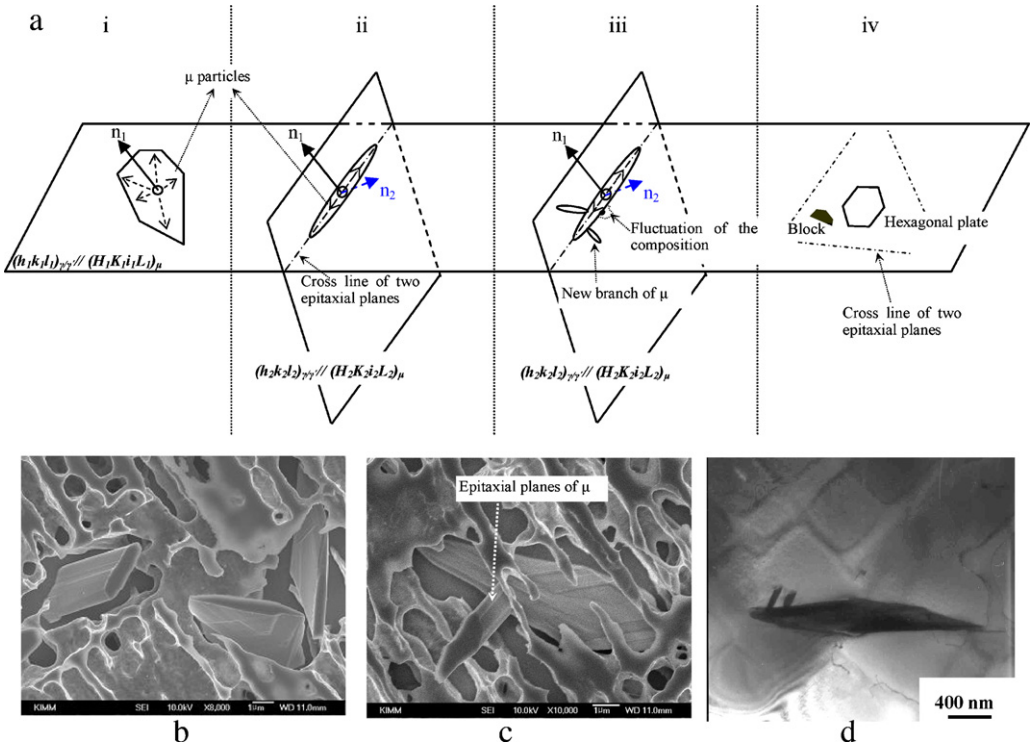

Fig. 10. (a) Schematic precipitation mechanisms of μ phase and SEM and TEM micrographs from (b) 1050 °C/3000 h showing growth of the μ phase based on mechanism ii, and from (c) 1050 °C/3000 h and (d) 950 °C/3000 h based on mechanisms iii.

since the different thickening rates in directions of n_1 and n_2 are different due to the different crystallographic growth preference;

(iii) In case of (ii), new branches may nucleate on the original rod due to the composition fluctuation in the surrounding matrix and grow based on their own epitaxial relationships into the matrix (Fig. 10c and d).

(iv) Finally, if the epitaxial growth of the μ phase is dependent on several low index planes of the matrix and its own which normal directions are not on a plane, morphology of the μ phase will be faceted blocky or hexagonal plate due to the limitation of spatial growth. The μ precipitates of this morphology are very universal in Simonetti's study [15].

Apparently, these low index planes are {0 0 1}, {0 1 1}, {1 1 2} or {1 1 1} for the matrix, {1 $\bar{2}$ 1 0} and {1 $\bar{1}$ 0 0} for the μ phase. Precipitation of the μ phase in the present study is mainly controlled by the mechanisms (ii) and (iii). The corresponding detailed morphologies of the μ particles are shown below the schematic mechanisms. It is worth noting that the obvious crystallographic planes which are parallel to the growth direction of μ particles may be the epitaxial planes (Fig. 10c). The TEM observation clearly shows two branches growing from the tip of a μ particle and good interfacial coherency between μ particle and the matrix along the side rather than in front of tips of the particles (Fig. 10d). Moreover, the growth directions are clearly shown to be the $\langle 1\,1\,0\rangle_{\gamma/\gamma'}$ according to surrounding γ′ position.

3.4. Creep properties

The creep properties at 1050 °C and 165 MPa of some exposed specimens are compared in Fig. 11a. The creep properties degraded with increasing thermal exposure temperature and time, while elongations of the thermally exposed specimens were larger than that of the specimen without thermal exposure. As stated previously, specimen 1# and 2# have similar amounts of μ phase (small), while specimen 3# and 4# have similar amount of μ phase (large). Another striking difference among these specimens is the extent of γ′ coarsening. Microstructural observations on longitudinal sections of the ruptured specimens show that cracks were exclusively concentrated in the interdendritic regions associated with micropores (Fig. 11b). More importantly, the μ phase showed good interfacial cohesion with surrounding γ′ phase and was free of crack (Fig. 11c) except specimen 4# in which some decohesion or crack initiation was found close to the μ phase but did not propagate into the γ′ envelope (Fig. 11d). Therefore, the μ phase might not further affect the creep properties of this alloy, except for depleting certain γ matrix strengthening elements such as W and Re. The short rupture lives and large elongations of the exposed specimens are mainly attributed to the coarsened γ′ phase [4,10]. Moreover, it is worth noting that, as shown in Fig. 11c, the needle-like μ particles transformed into small pieces which already coarsened (black arrows) and slightly deviated from the original direction of the needle like μ particles (white arrows). This implies that in the present case the μ phase may be under some transformation caused by the stress and γ′ coarsening during creep rather than be broken by stress concentration. Otherwise there would be cracks or decohesion close to these μ particles. The direction deviation of the μ phase may be due to the lattice distortion of the matrix caused by γ′ rafting [23], while the coarsening of the μ phase could be controlled by mechanism iv as proposed previously.

For specimen 4#, however, the creep rate was so high that there was not enough time for the transformation. Thus, due to their brittle nature the needle-like μ particles were fractured by the large creep deformation produced in the matrix. The further crack propagation during the tertiary creep stage is likely to have been confined due to other defects, such as interdendritic micropores, which are more sensitive to crack propagation as shown in Fig. 11b.

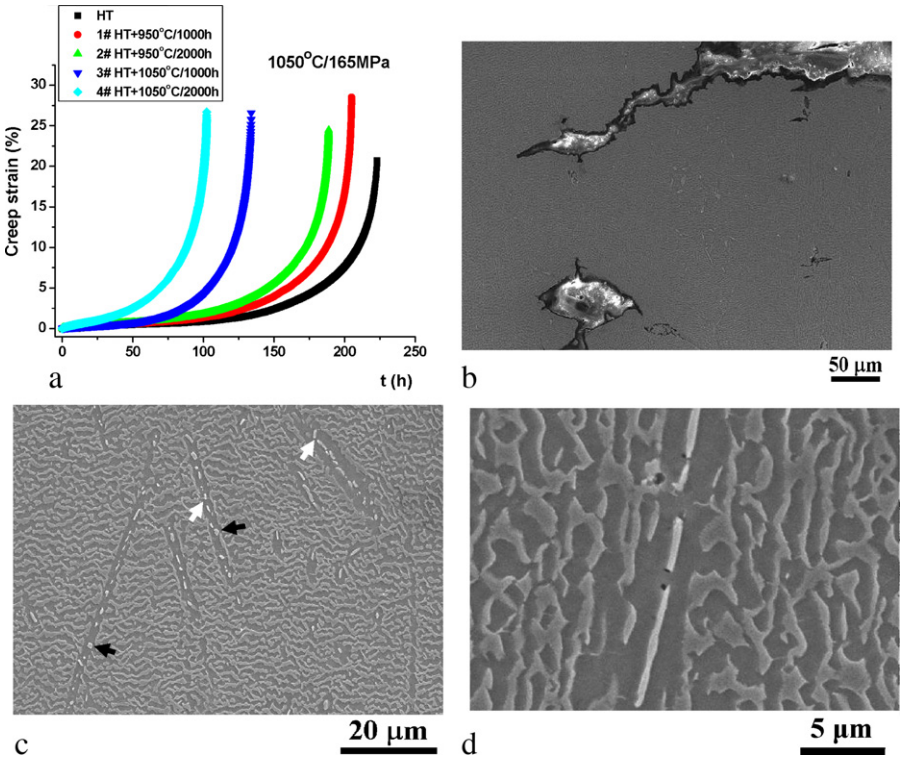

Fig. 11. (a) Creep properties of specimens with and without thermal exposure, and SEM micrographs of the longitudinal section fractured structures of (b) specimen 4# showing fracture due to propagation of cracks from interdendritic region, (c) specimen 2# showing rotated (white arrow) and coarsened (black arrow) μ particles free of crack and (d) specimen 4 showing crack initiation from the needle-like μ particle but without propagation.

4. Discussion

4.1. Effects of γ′ evolution on TCP formation

The γ′ evolution played a significant role in the precipitation behavior of μ phase during thermal exposure or during creep deformation. In modern superalloys the most typical feature is that the principal strengthening precipitates (γ′) has a much larger volume fraction than the matrix (γ). When exposed at high temperature the γ′ will coarsen or coalesce to its neighbors even without stress, which can inevitably affect the TCP phase formation.

Firstly, coarsening of the γ′ phase will lead to a decrease in the volume fraction of neighboring γ phase, which is equal to an increase of concentration of the TCP phase forming elements in γ [4]. Secondly, since the solution elements in γ and γ′ are different, when γ′ is coarsening, even if very slow, the different solution elements will be redistributed near γ/γ′ interfaces or will move in a certain way locally due to the chemical partition [24]. This regular movement or exchange of some solution elements such as W, Mo, Cr and Re may result in local segregation or clusters of these elements to some extent. Murakami et al. have predicted that the presence of Cr-W cluster in CMSX-4 alloy may be a sign of precipitation of a third phase such as TCP phase [25]. In addition, during thermal exposure, the interaction of different elements prevail so more clusters like the Cr–W cluster may form to provide fluctuations of composition and structure suitable for TCP phase nucleation. Since the γ′ coarsening and the subsequent movement and interaction of alloying elements are much faster at 1050 °C than that at 950 °C due to the different diffusion ability of alloying elements [20], more nucleation of the μ phase is produced earlier at 1050 °C. Moreover, it is well known that the μ phase usually forms at intermediate temperatures with some deviation depending on the compositions of alloys [8,15,16]. Therefore, once the μ phase has nucleated, it can grow relatively easily by attracting required elements from surrounding saturated matrix, which then becomes less dependent on the present test temperatures.

In addition, when coalescence of the γ′ phase occurs, the relative positions of γ matrix and the γ′ phase will be dramatically changed and even lattice distortion may occur [23], which may subsequently change the TCP phase morphologies as shown in Figs. 2 and 10b.

As we know the TCP phase forming elements such as Cr, Re, W and Mo have very low solubility and slow diffusive ability in the γ′ phase [4,20]. When TCP phases are surrounded by the coarsening and coalesced γ′ phase, they will show some stability due to the extreme difficulty of TCP phase forming elements to diffuse through the γ′ phase.

4.2. Role of the alloying elements

As given in the present study, the μ phase has a large composition range and is mainly composed of Ni, W, Re, Cr and Co. The equilibrium composition, which was obtained after certain thermal exposure time at respective temperatures, is consistent with Procter's work [18] in which the composition of μ phase is relatively constant, since the thermal exposure times were both over 1000 h at 1050 °C and 1150 °C in their study. There are high Ni content but low Re content in the μ phase at the beginning of thermal exposure because the diffusion rate of Ni is much higher than that of Re [20], which could also partly demonstrate that the growth rate of the μ phase at 950 °C is not much lower than that at 1050 °C.

In addition, it is interesting that the CMSX-4 alloy is relatively stable with respect to TCP formation, even though the contents of refractory elements such as Re, W and Cr are not low. This may be due to the very low content of Mo which is generally considered to cause alloy instability [4,8]. As shown in Rae's study, the distinct difference in composition between alloy 2071 and alloy CMSX-4 is the substitution of Mo for W in alloy 2071. However, the alloy 2071

is more prone to TCP phase formation and shows the presence of TCP phases of σ, μ, P and R in superalloys.

It is generally known that the Cr is prone to σ phase formation, W prone to μ phase, and Mo prone to μ phase and P phase [4,8]. However, although Re is generally thought to be prone to TCP phase formation and the content of Re was also found to be high in all the four common TCP phases in superalloys [8,10,12,13,26], it is still not clear that which specific TCP phase Re is prone to. Therefore, it is tempting to say that Re might mainly contribute to the composition of various TCP phases rather than to the type of them. The type of TCP phase might be determined by other refractory elements such as Cr, W or Mo. There was some evidence to this hypothesis in Feng et al.'s study in which the alloy UM-13, containing high content of Re but low content of other refractory elements, showed precipitation of δ-Re rather than TCP phases [26]. Moreover, Tian et al. found that the Re has an obvious effect on the precipitated μ phase and a large contribution to the composition [12]. Therefore, further study of the role of Re and the interaction between Re and other refractory elements in TCP phases formation is necessary, since it is directly related to the strength and stability of superalloys.

Although Ta and Ti have almost no contribution to the composition of the μ phase in the present study or of the TCP phases in elsewhere [8,10,16,24], they can lead to the chemical segregation in superalloys [4,8], and indirectly give rise to the microstructural instability in superalloys.

4.3. Preferable growth orientations of μ in γ/γ′

A previous TEM analysis of the crystallographic orientation relationships between the μ phase and the γ/γ′ matrix in MC2 superalloy showed that it may exist in five non-equivalent orientation relationships, each one corresponding to a particular precipitate shape: hexagonal platelet, rod or globular particle [27]. These orientation relationships may explain the simple morphology (most rod-like) of μ phase in the present study, since it only exists in two non-equivalent orientation relationships between μ phase and matrix. According to the solid state precipitation theory [22], this anisotropic growth of a precipitate is energetically promoted by a better coherency along the selected interfaces which were determined in present study as epitaxial planes of $\{0\,0\,1\}_{\gamma/\gamma'}$, $\{0\,1\,1\}_{\gamma/\gamma'}$, $\{1\,1\,2\}_{\gamma/\gamma'}$ and $\{1\,1\,1\}_{\gamma/\gamma'}$ or $\{1\,\bar{2}\,1\,0\}_{\mu}$ and $\{1\,\bar{1}\,0\,0\}_{\mu}$ as well as the preferential growth directions of $\langle 0\,0\,0\,1\rangle_{\mu}$ or $\langle 1\,1\,0\rangle_{\gamma}$ for μ phase. Moreover, it proved that, as shown in Fig. 9, these selected interfaces showed strong interfacial coherency, but the area in front of the tip did not, since the phase transformation mostly took place at the tip during growth of the μ phase.

This study revealed a relationship between the crystallographic orientation relationship and the growth manner of the μ phase with respect to the matrix, which can be supplementary to Procter's work [18]. Furthermore, several mechanisms for the precipitation behavior of the μ phase in superalloys have also been proposed. These both demonstrated the interfacial coherency between the μ phase and the matrix, which would lead to the difficulty of the crack initiation on the μ phase [15,16].

4.4. Role of the μ phase during creep deformation

It is reasonable that μ phase may not produce as much deformation as the matrix due to its brittle nature. Therefore, the fact that μ phase did not act as crack site or even fracture like specimen 1–3# in the present case, indicates that the μ phase has not been seriously deformed during creep. It is worth noting that the μ particles are mostly rod-like and are always surrounded by the γ′ envelope, on which the discussion concerning the role of the μ phase during creep deformation is based here. It is well known that at the beginning of creep, especially at high temperature and low stress, the dislocations mainly propagate and move in the γ phase and can hardly cut or climb into the γ′ phase, indicating little deformation in the γ′ phase. Correspondingly, the μ phase is not deformed and is under a relative uniform stress state rather than stress concentration due to the pile-up of dislocations. Moreover, the γ′ phase is also under stress coarsening in this stage and then may influence the morphology of the μ phase from elongated rods to small pieces. As shown in present study, the long rod-like μ particles already changed into short rods or small blocky ones. With the increase of creep rate, the γ phase cannot produce enough deformation and consequently considerable dislocations cut into the γ′ phase, which results in much deformation around the μ phase. In this case, the small pieces of μ particles can be considered as hard particles inside the γ′ matrix and dislocations may move in the γ′ phase by bypassing these μ particles. Therefore, these μ particles are free of cracks, which is also partly due to the strong interface coherency between them and the matrix.

However, in the case of specimen 4#, the creep rate noticeably increased since the beginning of creep (Fig. 11), which resulted in obvious deformation through both the γ and γ′ phases. Thus, in order to keep the deformation compatibility with the surrounding γ′ phase, the needle-like μ particles were fractured due to their brittle nature as well as the interfacial decohesion. In this case, the load transfer theory applied to the rupture of fibers in composite materials may be applicable as suggested by Simonetti and Caron [15]. Meanwhile, the other defects in the specimen, like micropores in interdendritic regions, were more sensitive than these γ′ surrounded μ particles in this condition. Therefore, role of the μ particles on the crack initiation process during the tertiary creep stage is probably limited because most part of the cracks were initiated on interdendritic micropores as in the single crystal superalloys free of TCP phase [15].

Role of the rod-like μ particles during the creep deformation is dependent on the creep rate which is closely related to the main strengthening γ′ phase. Therefore, compared to the γ′ evolution during thermal exposure or creep, effect of the rod-like μ particles by softening the γ phase or disturbing the γ/γ′ structure is very small on the creep properties of the CMSX-4 alloy. Moreover, the role of these μ particles during creep deformation may also be related to their morphologies and their positional relationship with the γ/γ′ phases. For example, if μ particles were large and plate-like, the γ′ phase may not completely envelop them. In this case, the dislocations in γ matrix may pile up on μ particles and lead to the stress concentration even at an early stage of creep, which would result in the early crack initiation around these particles.

5. Conclusions

The following conclusions can be drawn from this work:

(a) The γ′ evolution can affect the nucleation and growth morphology of the μ phase and even affect the fracture behavior of the μ phase during creep deformation.
(b) The μ phase is mainly composed of Ni, Cr, Co, W and Re. Contents of the Ni, W and Re has a large variation in the μ phase. High content of Ni but low content of W and Re at the early stage of thermal exposure is due to different atomic diffusion rates of these elements in the matrix, which can also explain the fewer limited growth of μ phase by forming thin layers at low temperature or at the early stage of thermal exposure.
(c) The μ particles nucleated and grew based on low index planes of both the μ phase ($\{1\,1\,\bar{2}\,0\}$ and $\{1\,0\,\bar{1}\,0\}$) and the matrix ($\{1\,1\,0\}$, $\{0\,0\,1\}$ or $\{1\,1\,1\}$ and $\{1\,1\,2\}$) by epitaxial growth

toward $\langle 0\,0\,0\,1\rangle_{\mu}$ or $\langle 1\,1\,0\rangle_{\gamma}$ directions, resulting in the predominantly rod-like morphology.

(d) Role of the rod-like μ particles during the creep deformation was dependent on the creep rate which was closely related to the main strengthening γ′ phase. The rod-like μ particles were not fractured by stress concentration. Their effect on the creep properties by softening the γ phase or by disrupting the γ/γ′ structure is much smaller compared to the dramatic γ′ evolution.

References

[1] Q. Zeng, S.W. Ma, Y.R. Zheng, S.Z. Liu, T. Zhai, J. Alloys Compd. 480 (2009) 987–990.
[2] C. Wang, J. Zhang, L. Liu, H. Fu, J. Alloys Compd. 508 (2010) 440–445.
[3] K.Y. Cheng, C.Y. Jo, T. Jin, Z.Q. Hu, Mater. Sci. Eng. A 528 (2011) 2704–2710.
[4] R.C. Reed, The Superalloys: Fundamentals and Applications, Cambridge University Press, 2006.
[5] J.B. le Graverend, J. Cormier, P. Caron, S. Kruch, F. Gallerneau, J. Mendez, Mater. Sci. Eng. A 528 (2011) 2620–2634.
[6] R. Rettig, R.F. Singer, Acta Mater. 59 (2011) 317–327.
[7] J.S. Hou, J.T. Guo, G.X. Yang, L.Z. Zhou, X.Z. Qin, H.Q. Ye, Mater. Sci. Eng. A 498 (2008) 349–358.
[8] C.M.F. Rae, Mater. Sci. Technol. 25 (2009) 479–487.
[9] A.I. Epishin, T. Link, H. Kingelhöffer, B. Fedelich, P. Portella, Mater. High Temp. 27 (2010) 53–59.
[10] J.J. Moverare, S. Johansson, R.C. Reed, Acta Mater. 57 (2009) 2266–2276.
[11] N.V. Petrushin, I.L. Svetlov, A.I. Samoylov, G.I. Morozova, Int. J. Mater. Res. 5 (2010) 594–600.
[12] S. Tian, M. Wang, T. Li, B. Qian, J. Xie, Mater. Sci. Eng. A 527 (2010) 5444–5451.
[13] J.Y. Chen, Q. Feng, Z.Q. Sun, Scr. Mater. 63 (2010) 795–798.
[14] D. Wang, J. Zhang, L.H. Lou, Mater. Sci. Eng. A 527 (2010) 5161–5166.
[15] M. Simonetti, P. Caron, Mater. Sci. Eng. A 254 (1998) 1–12.
[16] J.X. Yang, Q. Zheng, X.F. Sun, H.R. Guan, Z.Q. Hu, Scr. Mater. 55 (2006) 331–334.
[17] Y.F. Han, W.Y. Ma, Z.Q. Dong, S.S. Li, S.K. Gong, in: R.C. Reed, et al. (Eds.), Superalloys 2008, TMS, Warrendale, PA, 2008, pp. 91–97.
[18] C.S. Proctor, Formation and effects of intermetallics in the rhenieum-containing nickel-base superalloy CMSX-4, Ph.D. Thesis, University of Cambridge, 1993.
[19] U. Hemmersmeier, M.F. Kniepmeier, Mater. Sci. Eng. A 248 (1998) 87–97.
[20] C.E. Campbell, W.J. Boettinger, U.R. Kattner, Acta Mater. 50 (2002) 775–792.
[21] A.K. Sinha, Prog. Mater. Sci. 15 (1972) 81–185.
[22] C.N.R. Rao, K.J. Rao, Phase Transitions in Solids, McGraw-Hill Inc. International Book Company, 1978.
[23] T. Inoue, K. Tanaka, H. Adachi, K. Kishida, H. Inui, Adv. Mater. Res. 26–28 (2007) 213–216.
[24] J. Tiley, G.B. Viswanathan, R. Srinivasan, R. Banerjee, D.M. Dimiduk, H.L. Fraser, Acta Mater. 57 (2009) 2538–2549.
[25] H. Murakami, H. Harada, Y. Saito, J. Jpn. Inst. Met. 63 (1999) 723–732.
[26] Q. Feng, T.K. Nandy, T.M. Pollock, Mater. Sci. Eng. A 373 (2004) 239–249.
[27] M.P. Simonetti, P. Donnadieu, P. Caron, Scr. Metall. Mater. 30 (1994) 1553–1558.